Application of High Harmonic Fast Waves for Off-Axis Current Drive in the DIII-D and FNSF-AT Tokamaks

R. Prater[1], C.P. Moeller[1], R.I. Pinsker[1], M. Porkolab[1a], O. Meneghini[2], V.L. Vdovin[3]

[1]*General Atomics, P.O. Box 85608, San Diego, California 92186-5608, USA*

[2]*Oak Ridge Institute for Science Education, Oak Ridge, Tennessee 37830-8050, USA*

[3]*Kurchatov Institute, 1, Kurchatov sq., Moscow, 123182, Russia*

[a]*Permanent address: Massachusetts Institute of Technology, 77 Massachusetts Ave., Cambridge, MA 02139, USA*

Abstract. Fast waves at frequencies far above the ion cyclotron frequency and approaching the lower hybrid frequency (also called "helicons" or "whistlers") have application to off-axis current drive in tokamaks with high electron beta. The high frequency causes the whistler-like behavior of the wave power nearly following field lines, but with a small radial component, so the waves spiral slowly toward the plasma center. The high frequency also contributes to strong damping. Modeling predicts robust off-axis current drive with good efficiency compared to alternatives in high performance discharges in DIII-D and Fusion Nuclear Science Facility (FNSF) when the electron beta is above about 1.8%. Detailed analysis of ray behavior shows that ray trajectories and damping are deterministic (that is, not strongly affected by plasma profiles or initial ray conditions), unlike the chaotic ray behavior in lower frequency fast wave experiments. Current drive was found to not be sensitive to the launched value of the parallel index of refraction $n_{\|}$, so wave accessibility issues can be reduced. Use of a traveling wave antenna provides a very narrow $n_{\|}$ spectrum, which also helps avoid accessibility problems.

PACS Numbers: 52.35Hr

1. Introduction

Steady-state operation of a post-ITER tokamak like the Fusion Nuclear Science Facility-Advanced Tokamak (FNSF-AT) [1] or a power plant like ARIES-RS [2] requires that substantial off-axis current be driven by external power systems. Noninductive current drive is needed to complement the bootstrap current to support the plasma current in steady state. To obtain a large fraction of bootstrap current, the driven current must be off-axis to maintain a reverse (or negative) magnetic shear profile that supports stable operation at high beta, which is necessary for high fusion power density [2]. In order to reduce operating costs in FNSF, or to reduce the re-circulating power in an energetically efficient power plant, the fraction of plasma current not supported by the bootstrap current must be driven efficiently by external sources. Since current drive efficiency has an inverse dependence on density, higher current drive efficiency may also support an operating point at higher density for improved lifetime of the divertor.

In a series of experiments starting in the early 1980s, use of the slow wave for Lower Hybrid Current Drive (LHCD) demonstrated that high current drive efficiency [3] could be obtained in tokamak discharges with the low electron beta β_e $(= n_e kT_e / B^2 / 2\mu_0)$ characteristic of that period. The LHCD experiments, however, showed two effects that motivated a search for alternative current drive methods for larger, higher beta tokamaks. First, LHCD exhibited a density limit [3], above which effects related to the lower hybrid resonance cause a strong reduction in the power to the electrons. This density limit may interfere with the desired operating conditions for some experiments and for power plants. Second, at the high electron temperatures characteristic of reactors, modeling shows that the LH wave is damped on thermal electrons near the plasma boundary where

the electron temperature reaches 6 to 8 keV. For reactors, this may be near the top of the pedestal region, so the wave may not penetrate to the plasma core.

Fast waves at frequencies much larger than the ion cyclotron frequency, also called "whistlers" or "helicons" (terms used interchangeably here), have been suggested for driving the plasma current in DEMO [2,4,5] without the limitations of LHCD. These waves propagate into the plasma core without a density limit, and the weaker electron damping compared to the lower hybrid (slow) wave implies they may avoid full damping near the plasma boundary.

Experimental validation of this current drive process using fast waves at ion cyclotron harmonics of order 10 to 50 – that is, in the lower hybrid range of frequencies (LHRFs) – is not well developed. Several current drive experiments starting in the mid-1980s were performed using fast waves in the LHRF, including on JIPPT-IIU [6], PLT [7,8], and JFT-2M [9]. For an excellent discussion of these experiments, see reference [10]. The results of these experiments exhibited little difference between the fast wave and the slow LH wave [10]. In PLT, for example, the current drive using an array of dielectric-loaded waveguides launching the fast wave was very similar to that from LHCD using the same frequency and the same plasma parameters [7,8]. Most compelling was that the density limit found for LHCD was also found for the fast wave current drive, although the fast wave does not experience the lower hybrid resonance and should propagate to higher density. The widely accepted conclusion from these experiments is that mode conversion between the fast and slow waves near the plasma boundary was responsible for waves launched as fast waves to act like slow lower hybrid waves [10].

These experiments were performed in plasmas in which the damping on electrons [11,12] was weak. Weak damping implies that a ray may travel throughout the plasma, including traversing the low density edge where mode conversion is possible because both fast and slow waves propagate there [13]. Additionally, the waves were launched with low $n_{||}$, around 2, following the standard LHCD prescription that faster waves interact with faster electrons, thereby providing higher current drive efficiency [3]. However, low $n_{||}$ is also associated with greater likelihood of mode conversion near the launch location [13].

The present paper describes the benefits that follow from application of high frequency fast waves in plasmas with strong electron damping. This condition can be achieved in the DIII-D tokamak [14], so this device is considered here as a test bed in which the physics of high harmonic fast wave current drive in the strong single pass damping regime can be explored. In addition, the same computational tools are applied to driving current in the FNSF-AT [1]. These computations show that the high harmonic fast wave is significantly more effective at driving off-axis current than the alternatives.

The modeling results are consistent with the ray tracing calculations in reference [2] and the full wave calculations in reference [15], but greater detail is provided here. In addition, we show that the off-axis current drive is nearly independent of the launched $n_{||}$. This means that the wave can be launched with values of $n_{||}$ that are not subject to mode conversion to the slow wave. We also propose the use of a traveling wave antenna as an effective means to launch a narrow spectrum of $n_{||}$ and to reduce coupling problems associated with changing conditions in the plasma edge.

2. High Harmonic Fast Wave Current Drive

Fast waves at high cyclotron harmonics tend to propagate nearly along the magnetic field lines [16], but with also a small perpendicular (radial) component that causes the wave trajectories to spiral toward the magnetic axis. This trajectory means that the wave travels long distances in the off-axis region of the plasma. If the damping is sufficiently strong, the wave damping will take place off-axis, heating and driving current there.

The wave absorption in a warm Maxwellian plasma with electron density n_e and electron temperature T_e is via parallel Landau damping, given by [11,12]

$$k_{\perp i} = \frac{\sqrt{\pi}}{4} k_{\perp} \beta_e \xi_e e^{-\xi_e^2} G \quad , \tag{1}$$

where $k_{\perp}$ is the perpendicular wavenumber and $k_{\perp i}$ is its imaginary part, $\xi_e = v_{\|} / v_{te} = c / n_{\|} v_{te}$ where $v_{\|}$ is the phase velocity of the wave parallel to the magnetic field B, $v_{te} = \sqrt{2kT_e / m_e}$ is the electron thermal speed, $n_{\|}$ is the parallel index of refraction, and c is the speed of light. Here

$$G = \frac{n_{\|}^2 - S}{A_2} + \frac{\left[1 + \frac{\omega_{pe}^2}{\omega_{ce}^2} \frac{\mathrm{Re}(Y)}{|Y|^2} \frac{1}{n_{\|}^2 - S}\right] \left(\frac{mc^2}{kT_e}\right)^2 \frac{\omega_{ce}^2 D^2}{\omega^2 \left|\varepsilon_{33}^2\right|}}{A_1 A_2} \quad , \tag{2}$$

where ω_{pe} is the electron plasma frequency, ω_{ce} is the electron cyclotron frequency, ω is the frequency of the applied wave, and $\varepsilon_{33} = Y \omega_{pe}^2 / \omega^2$ is an element of the dielectric

matrix [16]. In equation (2), $Y = 2\xi_e^2\left[1+\xi_e Z\left(\xi_e\right)\right]$ and $Z\left(\xi_e\right)$ is the plasma dispersion function [17], and

$$A_1 = n_\parallel^2 - S + \frac{\omega_{pe}^2}{\omega_{ce}^2}\frac{\mathrm{Re}(Y)}{|Y|^2}\frac{n_\parallel^2}{n_\parallel^2 - S} \quad \text{and}$$

$$A_2 = n_\parallel^2 - S + \frac{\omega_{pe}^2}{\omega_{ce}^2}\frac{\mathrm{Re}(Y)}{|Y|^2}\frac{n_\parallel^2 + S}{n_\parallel^2 - S}.$$

Finally, the perpendicular wavenumber is given by

$$k_\perp = \frac{\omega}{c}\sqrt{\frac{\left(S - n_\parallel^2\right)^2 - D^2}{S - n_\parallel^2 + D^2\dfrac{\mathrm{Re}\left(\varepsilon_{33}\right)}{\left|\varepsilon_{33}\right|^2}\dfrac{n_\parallel^2}{\left(S - n_\parallel^2\right)}}} \quad . \tag{3}$$

In these equations, the quantities S and D are the well known Stix parameters [16] for a cold plasma.

The plasma parameters providing strong wave absorption can be understood from equation (1). Figure 1 shows contours of $0.2k_{\perp i}a$, where $k_{\perp i}$ is from equation (1) and a is the minor radius, for parameters characteristic of a high performance discharge in DIII-D that will be described later. When $0.2k_{\perp i}a$ is less than unity, the wave is absorbed in a small fraction of the minor radius. Figure 1(a) indicates that the desired strong absorption can be attained for any value of ξ_e only when β_e is above 1.8% and only for ξ_e below 2.8 for any reasonably realizable value of β_e. Figure 1(b) shows

contours of the same quantity plotted against applied frequency, showing that the frequency must be above 400 MHz.

3. GENRAY calculations for DIII-D

Calculations of heating and current drive for the high harmonic fast wave using the ray tracing code MRAYS and the full wave code PSTELION [5] have been performed by Vdovin [15] for representative DIII-D, ITER, and DEMO plasmas. In this paper, we apply primarily the GENRAY ray tracing code [18]. This code uses actual equilibria reconstructed from experiments, along with experimental measurements of plasma kinetic profiles. The ray tracing approach is a good approximation because the wavelength is small compared to the machine size at the high frequency being considered, and since only the strong single-pass damping situation is being considered, interference between rays may not be important because the rays don't travel far, and diffraction effects are probably small (although in full wave calculations with PSTELION [15] some reflection effects are observed in the interference patterns for large scale high beta plasmas). Ray tracing is very fast, allowing for practical parameter scans. Importantly, ray tracing yields information along the ray trajectory and this information can be used to develop a detailed understanding of the physics of the results. Ray tracing has its limitations as well. In the present study, the rays are started just inside the plasma ($\rho = 0.98$, where ρ is the square root of the normalized toroidal flux), so no information about the coupling of waves from the antenna to the plasma edge is developed.

The GENRAY code has many options for absorption and current drive. Here we use the model from Chiu [11], described above, for wave absorption on electrons, and for current drive the standard Ehst-Karney model [19] is used. At the high harmonics being

considered, the wave absorption by thermal ions is probably negligible, and the absorption on energetic ions like neutral beam ions in DIII-D or alphas in FNSF is not considered. Also, damping calculated for a Maxwellian ion distribution is likely not accurate for the slowing down distribution from neutral beam injection or alpha particles from nuclear fusion. However, we are interested in conditions where the wave never travels to normalized minor radii less than 0.5, so the interaction with the strongly peaked fast ions may not be too large. This is a topic needing further exploration.

For modeling purposes, a past DIII-D discharge with high normalized performance was chosen. This double null discharge in deuterium was characterized by excellent H-mode confinement, with confinement factor H98(y,2) [20] greater than 1.5, at the large value of normalized beta β_N ($=\beta aB/I_p$, where I_p is the plasma current in MA) of nearly 4. The time traces for this discharge are shown in figure 2. 9.4 MW of neutral beam injection (NBI) is applied, plus 1.85 MW of electron cyclotron heating (ECH) concentrated near r=0.68. The current density profile in this high performance discharge was obtained by ramping both the plasma current and the toroidal field, as shown in figure 2. These ramps generate Ohmic currents that provide the negative central magnetic shear shown in figure 3(a), or equivalently the equilibrium current density shown in figure 3(b). The current and field ramps end at about 3.3 s, and about 0.2 s later a large tearing mode with toroidal mode number n=1 and poloidal mode number m=2 appears. The tearing mode causes a large decrease in confinement, and all of the NBI power available is insufficient to maintain the feedback value of β_N. So this discharge is characterized by excellent performance, but the means to sustain the current profile that supported the performance were not available. Thus, the motivation for application of

high harmonic fast waves to this discharge is sustainment of the high performance already achieved by ramping. With present resources plus 1 MW of helicon power, DIII-D will still not have enough off-axis current drive power to sustain this plasma in steady-state at this density and current. But plasmas like this one can be used to study fast wave current drive under conditions where sufficient fast wave power could support high performance in steady-state.

Using GENRAY, the rays are launched as a bundle of starting angles, with the power in each ray adjusted to simulate a reasonable spectrum in the poloidal and parallel directions. In this study we used 18 rays, starting all rays at a single point representing the center of the antenna, with the poloidal angle spectrum centered at 0 and with width set by diffraction for an antenna height set to be 0.18 m. The $n_{||}$ spectrum was centered at 3.0 initially, with a spectral width of 10% and negligible power in the reverse spectrum. The antenna was placed at a poloidal angle of 45 deg--that is, 0.34 m above the midplane. The antenna concept will be described later in this paper. The applied frequency was 500 MHz and the nominal power was 1 MW. The electron density and temperature are as shown in figure 3(c,d).

The rays calculated by GENRAY spiral about the magnetic axis, although they propagate primarily along the magnetic field line. The poloidal projection of the trajectory of the central ray is shown in figure 4. The rays closely resemble the electric field patterns calculated by Vdovin for somewhat similar conditions but using a full wave code [15]. In figure 4 the width of the ray is proportional to the power deposition, so the spiral trajectory combined with the strong damping place nearly all the power off axis at

ρ around 0.5. The profiles of current and power calculated by GENRAY are shown in figure 5(a,b). As expected from figure 4, the current density and power densities are peaked around $\rho = 0.56$.

In total, 60.3 kA is deposited by 1 MW of fast wave power at 500 MHz with $n_{||}$=3.0. This current corresponds to a figure of merit $\eta \equiv n_e IR/P = 0.62 \times 10^{19}\ A/Wm^2$, or a dimensionless efficiency [21] of $\zeta \equiv e^3 n_e IR/\varepsilon_0^2 PkT_e = 0.64$, where I is the current driven by power P and R is the major radius. In evaluating these expressions, density and temperature at the r=0.5 surface, the approximate location of the current, are used.

A systematic study of the effect of launch location and choice of launched $n_{||}$ on the magnitude and location of the current drive shows that the choices made for figures 4 and 5 are close to optimum. This study used the OMFIT procedure [22] to systematically vary the launch location and $n_{||}$ value and run GENRAY for each case. In GENRAY the poloidal launch location is specified by the poloidal angle, which runs from 0 deg on the outboard midplane to 180 deg at the inboard midplane. The poloidal launch angle was varied over the range -80 deg to +80 deg in steps of 5 deg, thereby covering the full outer wall, while the $n_{||}$ was varied in steps of 0.1 from 2.0 to 4.0. The results, shown in figure 6(a) as contours of constant driven current per unit power and in figure 6(b) as contours of the normalized minor radius ρ of the peak in driven current. Here, the peak is defined as the radial location of the maximum of $j \times A$, where j is the driven current density in a radial bin and A is the area of the bin. Figure 6 shows that the chosen location and $n_{||}$ are consistent with the maximum driven current at the desired mid-radius

location. From the contours, a larger value of $n_{\|}$ would also work about as well, but discussion in Section 6 will show that coupling through a vacuum gap is easier with smaller values of $n_{\|}$; but on the other hand, if $n_{\|}$ is too small there may be problems with mode conversion to the outward bound slow wave [13]. Hence, $n_{\|}$=3.0 and launch angle of 45 deg are good compromise conditions.

The asymmetry in poloidal propagation direction follows from the whistle-like nature of the waves, which tend to follow field lines. Thus, the toroidal direction of launch and the magnetic helicity determine whether the rays travel clockwise or counter clockwise around the minor axis. Some control over the deposition location can be obtained by the choice of the toroidal field and plasma current direction.

From figures 1 and 4, the key to off-axis current drive is to have plasma conditions that keep the wave from traveling too fast toward the plasma center while having absorption sufficiently strong that the wave is fully damped before approaching the axis. These conditions can be estimated. The radial group velocity, in the propagating region and under the assumptions that ion motion may be neglected and that the wave velocity in the parallel direction is much larger than in the perpendicular direction, is given by $v_{g\perp} \approx c\left(\omega\Omega_e / \omega_{pe}^2\right) n_{\|}$ and the parallel group velocity is approximately $v_{g\|} \approx \left(c/n_{\|}\right)$. Defining the time the ray takes to travel to the axis $\tau_\perp = a / v_{g\perp}$, where a is the minor radius, and the time the ray takes to travel half-way around the minor circumference as it follows a field line $\tau_{\|} = \pi R_0 q / v_{g\|}$, the ratio $\left(\tau_\perp / \tau_{\|}\right) = \left(a/\pi R_0 q\right)\left(\omega_{pe}^2 / \omega\Omega_e n_{\|}^2\right) = 289\left(\varepsilon/\pi q\right)\left(n_{20} / f_{GHz} B n_{\|}^2\right)$ needs to be larger than

unity, where $\varepsilon = a / R_0$ is the inverse aspect ratio, n_{20} is the electron density in units of $10^{20}\,\mathrm{m}^{-3}$, f_{GHz} is the applied frequency in GHz, and q is the local safety factor. For values typical of tokamaks of $\varepsilon = 0.2$ and $q = 2$ at $\rho = 0.5$, keeping $\tau_\perp / \tau_\parallel > 1$ requires electron density $n_{20} > 0.1 f_{GHz} B n_\parallel^2$. For the DIII-D case, this means electron density above $5 \times 10^{19}\,\mathrm{m}^{-3}$.

For the condition on the electron temperature, consider that figure 1 shows that $\xi_e \approx 2$ locally (that is, irrespective of the launched value of $n_\parallel$) is the condition for strongest absorption. Here, $\xi_e = v_\parallel / v_t = c / n_\parallel v_t$. Using the relationship that $n_\parallel R$ is approximately conserved, where R is the major radius, the required electron temperature is $T_e \approx \left(511/2\xi_e^2 n_{\parallel a}^2\right)\left(R_0/R_0 + a\right)^2\,\mathrm{keV}$, where $n_{\parallel a}$ is the launched $n_\parallel$ near the outboard midplane at minor radius a. For $\xi_e = 2$ and $n_{\parallel a} = 3$, and for DIII-D $R = 1.7$ and $a = 0.6$, this gives an optimum electron temperature of above 3.8 keV. The requirement that β_e be larger than about 2% implies that for this electron temperature, the density must be above $3.3 \times 10^{19}\,\mathrm{m}^{-3}$ for toroidal magnetic field of 1.6 T. The condition that the radial propagation be not too rapid is more restrictive than the requirement on β_e when the condition on ξ_e is taken into account.

For comparison of current drive efficiency, the current driven by the heating systems currently available on DIII-D—neutral beam current drive (NBCD) and electron cyclotron current drive (ECCD)--can be calculated. For generating NBCD off-axis, one beamline on DIII-D was made so that it can be tilted in the vertical direction [23]. For the

maximum beamline tilt possible of 16 deg, and for the same equilibrium and plasma parameters as were used in the fast wave calculations, the maximum of the NBCD current density moves to $\rho = 0.42$, as shown in figure 7(a), according to calculations using the NUBEAM model [24]. In this calculation, the toroidal magnetic field and the plasma current direction were made so as to align the neutral beam with the local total magnetic field, which maximizes the NBCD. The beam accelerating voltage was 80 kV, which is consistent with the DIII-D power supplies, but which also is close to the limit set by beam shine-through. The beam ion species was deuterium. The total calculated NBCD driven is 26 kA/MW, or about half that calculated for the fast wave, and it has a much broader profile.

The alternate system for driving current in DIII-D is the ECCD system. The toroidal field of the equilibrium of figure 4, -1.6 T, is already very good for ECCD efficiency because the resonance intersects the $\rho = 0.5$ surface on the high field side, minimizing reduction of ECCD due to trapping of electrons in the magnetic well. The beam vertical launching angle was set to drive current peaking near a minor radius $\rho = 0.5$, and the toroidal angle was adjusted for maximum total ECCD. However, for the density profile of figure 3(c), the wave refraction is too large, so the density was reduced by 25% to allow access to the desired value of minor radius. Under this condition, the total driven current is 19 kA/MW, with the profile shown in figure 7(b). Correcting the driven current for the full density using constant η or ζ, the ECCD would be 15 kA/MW. This is only one quarter of the current driven by the high harmonic fast wave at the same power, although the peak J_{ECCD} value is higher than that from the fast wave owing to the very narrow profile, which is useful for MHD mode control using ECCD.

The results from the GENRAY model are well validated by similar calculations using a completely different physics model. The GENRAY model uses analytic forms for absorption [11] and current drive [19]. As a check on the physics of these models, a similar calculation was performed using the CQL3D Fokker-Planck code [25]. This code imports the ray trajectories and wave polarizations from GENRAY and calculates the flux in velocity space driven by the wave fields [16]. This flux is used as the source term in the Fokker-Planck equation, which is then solved at each point along the rays. Thus, the absorption and current drive can be calculated completely independent of the GENRAY model.

CQL3D shows that quasilinear effects are playing a minor role in the current drive. Current density profiles from CQL3D for three power levels are shown in figure 8, along with the GENRAY result from figure 5(a). The integrated current from CQL3D is 69.5 kA/MW for 0.1 MW of incident power, 66.4 kA/MW for 1 MW, and 57.5 kA/MW for 10 MW, compared to 60.3 kA/MW for the linear (power independent) GENRAY code.

The CQL3D calculations also identify the region of velocity space involved in the wave/particle interaction. Figure 9(a) shows the flux in normalized velocity space ($v_\perp / v_{te}, v_\parallel / v_{te}$) generated by the wave electric fields from 1 MW of incident power acting on the electrons, at the flux surface of maximum driven current density. This flux is the source term in the Fokker-Planck equation. Figure 9(a) shows that the interaction is with a small range of phase space with $v_\parallel / v_{te}$ between 2 and 2.3 and $v_\perp / v_{te}$ between 0 and 1. Figure 9(b) shows the logarithm of the total flux in velocity space, including the

collisional relaxation. The logarithm loses apparent information about the magnitude of the fluxes, but it clearly shows the vortices that are set up by the rf fields. Vortices are a necessary consequence of a forced flux in one part of velocity space because the total flux must be divergence free everywhere, in steady-state.

The deviation of the electron distribution function from a Maxwellian is quite small at power levels around 1 MW, as seen in figure 9(c). For 10 MW of power CQL3D indicates visible deviations from Maxwellian in the region of velocity where the interaction takes place, around $u_{\|} / v_{norm} = 0.25$ as shown in figure 9(d). The large apparent deviations from circles shown in the outer contours are probably not important from the point of view of current generation since the electron density (in phase space) there is so low. The fifth contour from the outside in figure 9(d) represents 10^{-8} of the peak density, while the contour at $u_{\|} / v_{norm} = 0.25$ is 10^{-2} of the peak density. It appears that the deviations from Maxwellian shown in figure 9(d) must be related to the small changes in the current density profile at 10 MW compared to 1 MW.

4. Sensitivity of GENRAY calculations to plasma parameters

The calculations shown in section 3 are for a discharge with pressure near the stability limit. This raises the question of how the helicon current drive varies if the plasma pressure is smaller. To address this, a sequence of GENRAY calculations was done with different electron density and temperature profiles. In each case, the profiles were simply scaled uniformly from those shown in figure 3, using the same equilibrium flux surfaces. The central electron density was scaled from 10.3 to 8.0, 6.0, and 4.0 in units of 10^{19} m^{-3}, with central electron temperature fixed at 3.48 keV; the central electron

temperature was scaled from 3.48 to 3.0, 2.75, 2.5, and 2.25, with the density fixed at 10.3; and then both density and temperature were scaled with the following pairs: (10.3, 3.48), (8.0, 4.5), (6.0, 6.0), (8.0, 3.0), (7.0, 2.75), and (6.0, 2.50).

The results of this scaling study show that a constant value of the dimensionless efficiency accurately describes the driven current for all the conditions tested. This behavior is shown in figure 10(a), in which the driven current per unit power is plotted as a function of T_e / n_e. The straight line is for constant dimensionless efficiency of 0.64, and all the data points lie close to it. Figure 10(b) shows that the minor radius of the peak of the driven current is a weakly increasing function of β_e for β_e above 1.5%, but that the minor radius drops rapidly at lower β_e. As β_e decreases, the rays tend to propagate further toward the magnetic axis, depositing current at smaller minor radius.

A more surprising result comes from a scan of $n_{||}$, shown in Table 1. This table shows that for a broad range of launched $n_{||}$ the driven current and the location of its peak as calculated by GENRAY are nearly constant. This is surprising because LHCD is quite sensitive to $n_{||}$, with low values associated with high current drive since the interaction is with more energetic, therefore less collisional, electrons. But for the helicon the driven current is essentially constant for launched $n_{||}$ between 2.8 and 4.2, and the minor radius where the current is peaked also is constant. For values of launched $n_{||}$ below 2.7 the absorption falls, apparently because ξ_e in equation 1 becomes too large; either a larger electron temperature or a larger geometric upshift in $n_{||}$ is required for good absorption. Absorption is marginal for an $n_{||}$ of 2.8, and part of the current is driven on-axis, giving an increase in the total current drive.

The weak scaling of the current drive with $n_{\|}$ can be understood from the data calculated by GENRAY at each point along the ray. Figure 11 shows parameters as a function of ray length for two values of launched $n_{\|}$, namely 3.0 and 4.0. As the ray propagates from the edge to the interior of the plasma, the local electron temperature increases. At the same time, the value of $n_{\|}$ also increases, due primarily to the geometric effect of decreasing major radius. This behavior is shown in the top boxes of figure 11. The ray propagates for a distance without absorption, then the absorption increases, peaks, and falls as the power in the ray is depleted. This is shown in the middle boxes of figure 11. The dotted vertical line indicates the location along the ray of the peak in power deposition. The value of $\xi_e = v_{\|} / v_{te} \propto \left(n_{\|}\sqrt{T_e}\right)^{-1}$ decreases as the ray propagates due to the increases in both the $n_{\|}$ and the electron temperature. Figure 11 shows that the absorbed power per unit ray length $-dP/ds$ becomes greater than zero when $\xi_e \approx 3$ and peaks where $\xi_e \approx 2$ or a little greater. This behavior is the same whether the initial value of $n_{\|}$ is 3.0 or 4.0, consistent with the absorption contours of figure 1.

The independence of the absorption and current drive location and magnitude on $n_{\|}$ is a result of the nature of the wave propagation and strong single pass damping of these high harmonic fast waves. The helical propagation depends only weakly on the value of $n_{\|}$, so the wave trajectories are not much affected, thereby defining the radial location of the interaction and the electron temperature. The absorption takes place where ξ_e has a suitable value, peaking at $\xi_e \approx 2$, and the magnitude of the current drive is determined by the absorption rate and the value of ξ_e [19].

This rather deterministic behavior of the rays in the high harmonic range of 30 to 50 can be contrasted with the more chaotic behavior of rays in the harmonic range of 5 to 10, characteristic of past experiments with fast waves in DIII-D in the 60-90 MHz range [26]. For the same equilibrium and profiles of figures 4 and 5 and using 90 MHz, the GENRAY calculations show full wave absorption by fast beam ions at the first cyclotron harmonic the ray encounters (the 9th harmonic). If the fast ion density is reduced from $4\times10^{18}\,\mathrm{m}^{-3}$ by a large factor, say 10^6, then the waves are fully absorbed by thermal ions at the same cyclotron harmonic. This absorption on thermal ions can be avoided computationally by reducing the ion temperature from 7 keV to a low value, say 1 keV. Then, with only electron absorption possible, the rays have to propagate a potentially long distance until they approach the center of the plasma with coincidentally a suitable value of $n_{||}$. During the long propagation distance, the $n_{||}$ of the ray varies wildly, going from the launched value of 3.0 to as large as 5 and as small as -5 (e.g., see reference [27]). For the conditions of discharge 122976, the damping length on electrons rarely, if ever, approaches the minor radius, as expected from figure 1(b). In any event, fast wave current drive at lower frequency will not be off-axis nor as well constrained as at the higher frequency.

5. GENRAY calculations for FNSF

An important motivator for helicon research is the need for a current drive mechanism of sufficiently high efficiency that it can support the desired current profile in a steady-state FNSF [1]. Lower hybrid waves tend to be damped near the top of the pedestal in such devices, typically at $\rho > 0.9$. ECCD, even when optimized, is marginal in efficiency [28]. Current drive with higher efficiency may permit operation of the FNSF

at higher density, reducing the tension between lower density for adequate current drive efficiency, and hence improved power balance, and higher density for greater survivability of the divertor.

The model FNSF double null equilibrium used here, shown in figure 12, was developed by V.S. Chan and A.M. Garofalo [1] for establishing a true steady-state. The plasma current is 6.6 MA, the toroidal field is -5.44 T, the major radius is 2.7 m, and the ion species are equal densities of tritium and deuterium, with a small minority of alpha particles (0.7% on axis of the electron density) and sufficient but small carbon impurity to provide an overall Z_{eff} of about 1.6. In the model used here the ion species mix does not affect the results. The kinetic profiles and the safety factor profile are shown in figure 13.

A brief survey of frequency and launched $n_{\|}$ has shown that 1.2 GHz is an appropriate frequency, corresponding to about the 30th harmonic of deuterium at the plasma center. Using this frequency and $n_{\|}$ of 2.2, the driven current is 37.7 kA/MW with a peak at $\rho = 0.62$, as shown in figure 14. The dimensionless current drive efficiency is $\xi = 0.76$ and the figure of merit is $\eta = 2.1 \times 10^{19}$ A/W/m^2, both of which are very high for off-axis current drive. Using the Fokker-Planck code CQL3D rather than GENRAY produces similar results, 34.9 kA, also shown in figure 14. Again, the current to power ratio was the nearly same for power of 100 MW, indicating that quasilinear effects are not significant.

By comparison, a study [28] of the optimization of ECCD in the same FNSF equilibrium showed significantly smaller efficiency. In this study, the EC source

frequency and the antenna location were considered free parameters that were systematically varied to find the largest driven current per unit power. The largest ECCD efficiency, $\xi = 0.42$ at $\rho = 0.6$, was found for a top launch of 200 GHz power in which the EC beam was directed nearly parallel to the cyclotron resonance so that a large Doppler shift could be enforced and the wave/particle interaction would therefore be with energetic electrons. This optimized approach is strongly affected by small changes in the toroidal field. A more conventional and flexible approach would put the EC launcher on the low field side, but then the dimensionless current drive efficiency is only $\xi = 0.27$ at the same value of ρ. The helicon current drive is much more efficient than either approach with ECCD.

A scan of $n_{||}$ for FNSF showed little sensitivity of the total driven current, much as in the DIII-D scan. Table 2 shows the current drive for values of launched $n_{||}$ between 1.8 and 3.2. The driven current drops off at $n_{||}$ above 2.6. This is because the slower the wave phase velocity at the antenna, the lower the electron temperature can be where the electrons begin damping the wave. This shifts the location where power is absorbed closer to the antenna, which means that the wave/particle interaction takes place at larger major radius and hence with greater trapping of electrons in the magnetic well, reducing the current. For $n_{||}$ between 1.8 and 2.6, the current varies less than 10%.

The reason for the weak dependence of current on launched $n_{||}$ is the same for FNSF as for DIII-D. Figure 15 shows the same data for the central ray for FNSF as figure 11 shows for DIII-D, except that the launched $n_{||}$ is 1.8 on the left and 2.6 on the right. Again, as the ray propagates with slowly decreasing minor radius, the $n_{||}$ slowly

increases due primarily to geometric effects. As the value of ξ_e approaches 2, the absorption becomes strong. Table 3 shows the parameters along the central ray where the absorption peaks for both the FNSF and DIII-D cases. In all cases the value of ξ_e is close to 2.0, even though the other parameters may be quite different.

6. Launching the helicon

Considerations of the launching of the fast wave lead to preferring a low value of $n_{||}$, for two reasons. First, the fast wave is evanescent at very low densities near and outside the plasma boundary. Typically, there is a minimum vacuum gap between the plasma boundary and the wall or antenna, else plasma performance suffers and material objects closer may be damaged by the heat flux from the plasma. The characteristic length L_a over which the electric field decays is related to $n_{||}$ through the expression $L_a = \lambda_0 \big/ 2\pi\sqrt{n_{||}^2 - 1}$, where $\lambda_0 = 2\pi c/\omega$ is the free space wavelength. The radial Poynting flux is proportional to the electric field squared, so the evanescence distance is half of L_a. The larger the value of $n_{||}$, the more strongly the fields are attenuated in the vacuum region near the antenna. Second, smaller $n_{||}$ means that the radiating elements are further apart, which helps to reduce the local electric fields that can cause electrical breakdown at the antenna. Figure 6(a) shows that a poloidal angle for the antenna location of 45 deg is a good choice for DIII-D in terms of high driven current at a relatively large minor radius. The figure also shows that for this poloidal angle, $n_{||}$ of 3.0 is as small as it can be made without sacrificing current drive efficiency. For these reasons, $n_{||}$=3.0 was used as the base case for the modeling calculations. Then the falloff distance for power is $L_a/2 \approx 1.7$ cm.

There is another limit on $n_{||}$ having to do with wave accessibility [29, summarized in 30]. This work has shown that there is a critical value of $n_{||}$ below which the inward traveling fast wave transforms in the plasma edge to an outward traveling slow wave, and the effect is to prevent the fast wave from accessing the plasma core. The critical $n_{||}$ for wave accessibility is given by the expression

$$n_{||} > n_{||crit} \equiv \left[1 - \left(\frac{\omega^2}{\omega_{ce}\omega_{ci}}\right)\right]^{-1/2} , \qquad (4)$$

which for the conditions of DIII-D is about 2.1 and for FNSF is about 1.23. So to avoid accessibility limits and mode conversion to the slow wave, the antenna should avoid having significant power in the part of its $n_{||}$ spectrum approaching or below $n_{||crit}$.

The combline traveling wave antenna (TWA) is an appropriate technology for launching a fast wave traveling in one toroidal direction in the plasma [31]. The combline consists of a toroidal sequence of passive radiating elements excited by a driven element at one end. The reactive mutual coupling between a radiating element and its neighbor and between the element and the Faraday screen and to a lesser extent with the plasma produce a traveling wave with a narrow spectrum of $n_{||}$. If the combline has a sufficient number of elements (*i.e.,* sufficient length in the toroidal direction) that most of the power is transferred to the plasma, then reflection from the end is avoided and the antenna can appear as a resistive load matched to the impedance of the transmission line.

The combline antenna has advantages over fast wave antennas in which each radiating element is individually excited by an external feed. Loading and power transfer

to the plasma is only weakly sensitive to the antenna-plasma gap for the combline antenna, making it suitable for H-mode plasmas with ELMs. In fact, the traveling wave aspect of the combline works best when the loading per element is not too strong, so that a large number of elements are engaged in defining the $n_{||}$ spectrum. Additionally, the gap allows the short wavelength evanescent power from non-ideal effects to decay before reaching the plasma. Weak damping can be compensated by making the antenna longer in the wave direction or by recirculating power remaining at the end back to the feed. The voltage at the feed may be smaller than that of antennas with individually fed elements because the combline appears as a matched resistive load, while individually fed elements are typically part of a resonant circuit. For example, for 1 MW of power the peak voltage in a 50-Ohm coaxial feed is less than 10 kV. The antenna can be compact, because the vertical (poloidal) dimension of the antenna can be made significantly less than half the free space wavelength; for 500 MHz, this is 30 cm. The combline antenna also has large advantages over an array of dielectric loaded waveguides [7,32] since loaded waveguides are difficult to make and would be very challenging to cool in a reactor environment.

A 12-element combline antenna has been tested experimentally in the JFT-2M tokamak [33,34] at 200 MHz. In these experiments, the combline antenna exhibited the expected characteristics. The input impedance maintained a good match to the impedance of the transmission line for all plasma loads including H-mode, L-mode, Ohmic, and vacuum (for preionization) conditions [33]. The antenna was operated reliably at power up to the available power, 400 kW, without exhibiting a power handling limit. Measurements of the wave electric field in the plasma core were consistent with full

wave calculations, indicating that the unidirectional fast wave was successfully launched [34]. In these experiments the wave damping was weak, and driven currents were not detected, but the launching of the fast wave was found successful.

The $n_{||}$ spectrum of a combline antenna suitable for DIII-D of length 1.8 m can be very narrow, as shown in figure 16. Small sidebands are present in the vacuum case, but no significant power is launched in the negative part of the spectrum. For the case of 90% of the power damped, the spectrum is broadened slightly, but the sidebands nearly disappear. Note that almost no power is radiated at $n_{||}$ anywhere near $n_{||crit}$ (=2.1), thereby providing some cushion in avoiding mode conversion.

7. Summary

Modeling with a ray tracing code and a Fokker-Planck code show that very high harmonic fast waves can drive off-axis current in tokamaks under suitable plasma conditions. One condition is that the wave frequency be sufficiently high that the wave acquired the whistler-like property of propagating nearly along a field line, giving the wave trajectories a spiral character. A second condition is that the density be sufficiently high that the radial propagation of the waves at roughly the Alfven speed is not too fast compared with the damping rate, and an estimate of the minimum density was derived. A third condition is that the wave absorption be sufficiently strong that the wave is fully damped before it reaches the magnetic axis. This condition requires electron temperature sufficiently high that the thermal velocity is about half the local parallel phase velocity of the wave, where the parallel phase velocity is determined from the launched parallel velocity and geometric factors. The wave absorption is also proportional to the electron beta and the frequency, so high frequency, high density, and high electron temperature

improve the damping. Taken together, the local electron beta must be above 1.8% for sufficient damping.

Scans of density, temperature, and launched $n_{||}$ for the DIII-D example show that the off-axis current drive scales with constant dimensionless efficiency, provided the electron beta is sufficiently high. The mechanistic behavior of the ray trajectories and $n_{||}$ evolution along the rays, along with the condition described above that $v_{||} / v_{te} \approx 2$ at the absorption location, implies that the total driven current is not very sensitive to the launched $n_{||}$, as shown by the scans. The launched $n_{||}$ spectrum can then be chosen for reasons having to do with avoiding mode conversion to the slow wave at the plasma edge and design of an effective antenna. The traveling wave antenna is a good option for launching the wave with a very narrow $n_{||}$ spectrum, simple feed, and low electric field.

The ray tracing model applies well developed and accepted physics models for wave propagation and absorption and current drive. The Fokker-Planck results validate the absorption and current drive using a different model. For the sample DIII-D case, the off-axis current drive is 2 to 4 times more efficient than off-axis neutral beam current drive or electron cyclotron current drive under the same conditions. For the FNSF case, the helicon current drive is similarly more effective than the alternatives evaluated to date.

Acknowledgement

This work was supported in part by the U.S. Department of Energy under DE-FC02-04ER54698 and DE-AC05-06OR23100.

References

[1] Chan, V.S., Stambaugh, R.D., Garofalo, A.M. *et al*. 2011 *Nucl. Fusion* **51** 083019

[2] Jardin, S.C., Kessel, C.E., Bathke, C.G. *et al*. 1997 *Fusion Eng. Design* **38** 27

[3] Gormezano, C. 1986 *Plasma Phys. Controlled Fusion* **28** 1365

[4] Koch R., Lerche E., Van Eester D., and Nightingale M. 2011 *Radio Frequency Power in Plasmas, Proc. 19th Topical Conf., Newport, RI (AIP, Melville, NY)* 349

[5] Vdovin, V.L. 2001 "3D full wave code modeling of ICRF plasma heating in large stellarators," *28th European Conf. on Controlled Fusion and Plasma Physics (Madeira, Portugal, 2001)* poster 4.058 (ECA) Vol 25A 1541

[6] Ohkubo K., Hamada Y., Ogawa Y. *et al*. 1986 *Phys. Rev. Lett.* **56** 2040

[7] Pinsker, R.I. 1986 *Fast Wave Current Drive Experiments on the Princeton Large Torus, Ph.D. Thesis, Princeton University*

[8] Pinsker, R.I., Colestock, P.L., Bernabei, S. *et al*. 1987 *Applications of Radio-Frequency Power to Plasmas, 7th Topical Conf., Kissimmee, FL (AIP, Melville, NY)* 175

[9] Uesugi, Y., Yamamoto, T., Hoshino, K. *et al*. 1987 *Proc. 14th European Conf. on Controlled Fusion and Plasma Physics (Madrid, 1987),* vol. **11D**, *Part III (EPS)* 942

[10] Pinsker, R.I. 1994 *Radio Frequency Power in Plasmas, Proc. 10th Topical Conf., Boston, MA (AIP, Melville, NY) 179*

[11] Chiu, S.C., Chan, V.S., Harvey, R.W., and Porkolab, M. 1989 *Nucl. Fusion* **29** 2175

[12] Porkolab, M. 1992 *Radio Frequency Power in Plasmas, Proc. 9th Topical Conf., Charleston, SC (AIP, Melville, NY) 197*

[13] Porkolab, M. 1985 *"Lower hybrid heating experiments in tokamaks: An overview," Course and Workshop on Applications of RF Waves to Tokamak Plasmas, Varenna, Italy, 1985* (Bernabei, S., Gasparino, U., Sindoni, E., Eds), *EUR 10333 EN,* ***1*** 288

[14] Luxon, J.L. 2002 *Nucl. Fusion* **42** 1813

[15] Vdovin V.L. 2013 *Plasma Physics Reports* **39** 95

[16] Stix, T.H. *Theory of Plasma Waves, 2nd ed. (Wiley, New York, 1992)*

[17] Fried, B.T., and Conte, S.D. *The Plasma Dispersion Function* (*Academic Press, New York, 1961*)

[18] Harvey, R.W., and Smirnov, A.P. 2001 *The GENRAY Ray Tracing Code*, CompX Report CompX-2000-01

[19] Ehst, D.A., and Karney, C.C. 1991 *Nucl. Fusion* **31** 1933

[20] *ITER Physics Basis*, 1999 *Nucl. Fusion* **39** 2208

[21] Luce, T.C., Lin-Liu, Y.R., Harvey, R.W. *et al.* 1999 *Phys. Rev. Lett.* **83** 4550

[22] Meneghini, O. and Lao, L. 2013 *Plasma Fusion Res.* **8** 2403009

[23] Murphy, C. *et al.* 2011 *SOFE: Proc. of the 24th Symp. on Fusion Engineering* (Chicago, IL, 2011) doi:10.1109/SOFE.2011.6052323

[24] Pankin, A. *et al.* 2004 *Computer Physics Communications* **159** 157

[25] Harvey, R.W., and McCoy, M.G. *The CQL3D Fokker-Planck Code*, 1992 *Proc. IAEA TCM on Advances in Simulation and Modeling of Thermonuclear Plasmas, Montreal, Canada*

[26] Petty, C.C. *et al.* 2001 *Plasma Phys. Controlled Fusion* **43** 1747.

[27] Prater, R., Austin, M.E. and Baity, F.W. *et al.* 1997 *Proc. 16th Int. Conf. on Fusion Energy, Montreal, 1996,* Vol 3, p 243

[28] Prater, R., Chan, V., and Garofalo, A. 2012 *Bull. Am. Phys. Soc.* **57** 188

[29] Golant, V.E. 1980 *Sov. Phys. Tech. Phys.* **16** 1980

[30] *Fusion Physics*, 2012, Eds. M. Kikuchi, K. Lachner, and Minh Quang Tran, Chapter 6 (IAEA, Vienna)

[31] Moeller, C.P., Gould, R.W., Phelps, D.A., and Pinsker, R.I. 1994 *Radio Frequency Power in Plasmas, Proc. 10th Topical Conf., Boston, MA,* (AIP, Melville, NY) 323

[32] Theilhaber, K., and Bers, A. 1980 *Nucl. Fusion* **20** 547

[33] Pinsker, R.I., Moeller, C.P., Petty, C.C. *et al.* 1997 in *Fusion Technol.* (Elsevier Science, Amsterdam, 1997) 629

[34] Ogawa, T., Hoshino, K., Kanazawa, S. *et al.* 2001 *Nucl. Fusion* **41** 1767

List of Tables

Table 1. Scan of fast wave current drive for a range of launched $n_{\|}$ for the DIII-D test case. Central density is 1.03×10^{20} m^{-3} and central T_e is 3.48 keV.

$n_{\|}$ (a)	CD (kA/MW)	ρ of peak j
2.8	68.8	0.56
3.0	60.3	0.56
3.2	58.7	0.54
3.4	58.7	0.54
3.6	59.4	0.55
3.8	59.7	0.55
4.0	59.4	0.57
4.2	58.2	0.60

Table 2. Launched $n_{\|}$, driven current, and location of the current peak, for the FNSF equilibrium of figures 12 and 13.

$n_{\|}$ (a)	CD (kA/MW)	ρ of peak j
1.8	35.7	0.62
2.0	37.5	0.62
2.2	37.7	0.64
2.4	35.9	0.67
2.6	33.3	0.69
2.8	30.6	0.71
3.0	28.2	0.72
3.2	26.1	0.73

Table 3. Parameters of the central ray at the location of peak absorption rate, for two $n_{||}$ values each for FNSF and DIII-D. The last row is the normalized power remaining in the ray.

	FNSF, $n_{||}$(a)=1.8	FNSF, $n_{||}$(a)=2.6	DIII-D, $n_{||}$(a)=3.0	DIII-D, $n_{||}$(a)=4.0
ρ	0.60	0.69	0.54	0.51
T_e(keV)	8.9	7.5	2.9	3.0
$n_{||}$	2.61	2.67	4.64	4.66
ξ_e	2.05	2.19	2.02	1.99
P	0.51	0.57	0.60	0.51

Figure Captions

Fig. 1. (a) Contours of $0.2k_{\perp i}a$ as a function of β_e and ξ_e, from equation (1). The electron density is fixed at 0.5×10^{20} m^{-3}, the toroidal magnetic field is $B_T = 1.6$ T, and the applied frequency is 500 MHz. (b) Contours of the same quantity as a function of applied frequency and ξ_e, with β_e fixed at 2.0%.

Fig. 2. (a) Plasma current, (b) toroidal field, (c) normalized beta, (d) confinement factor H98(y,2), and (e) neutral beam and ECH powers, for DIII-D discharge 122976. The vertical line is at 3.021 s, where much of the analysis of this paper is made. The plasma current is 1.57 MA and the toroidal field is -1.51 T at that time.

Fig. 3. Radial profiles of (a) safety factor q, (b) total current density from the equilibrium reconstruction, along with the calculated bootstrap current density, the neutral beam current density, and the electron cyclotron current density, (c) electron density and fast beam ion density (x10), and (d) ion and electron temperature and Z_{eff}, for DIII-D discharge 122976 at 3.021 s.

Fig. 4. Poloidal cross section of DIII-D discharge 122976 at time 3.021 s. The plasma current is 1.5 MA, the toroidal field is -1.51 T, the central electron density is 1.03x10^{20} m^{-3}, and the central electron temperature is 3.48 keV. The vertical lines are the cyclotron harmonics of deuterium, and the central ray is shown for 500 MHz and $n_{||}$=3.0. The thickness of the central ray is the proportional to the power deposition per unit ray length as calculated by GENRAY.

Fig. 5. (a) The profile of driven current density and (b) profile of electron heating density for the case of figure 4. The full power is absorbed and the driven current from GENRAY is 60.3 kA/MW.

Fig. 6. (a) Contours of total driven current, and (b) contours of the normalized minor radius where the driven current peaks, as a function of the poloidal angle of the launcher and the value of launched $n_{||}$. The black square shows the poloidal angle and $n_{||}$ used in the calculations in figures 4 and 5.

Fig. 7. (a) Current density driven by a tilted neutral beam, as calculated by the NUBEAM code. The accelerating voltage is 80 kV, the beam ion species is deuterium, and the beam tilt is 16 deg. The total driven current is 26 kA/MW. The plasma equilibrium and parameters are the same as for figure 5. (b) Current density driven by ECCD for the same equilibrium and parameters as for figure 5, except the density is reduced by 25% to allow the EC beam to intersect the resonance without very large refraction. The applied frequency is 110 GHz and the launch point is 0.69 m above the midplane.

Fig. 8. Radial profile of current density calculated by the Fokker-Planck code CQL3D and the linear code GENRAY. The total driven current is 66.4 kA/MW for CQL3D and 60.3 kA/MW for GENRAY. For CQL3D, current densities per MW for 0.1 MW and 10 MW are also shown.

Fig. 9. Phase space calculations by CQL3D for the case of figure 8. (a) The arrows represent the flux due to the wave electric fields acting on the electrons. The length of the arrow is proportional to the flux and indicates the direction. (b) The length of the arrow is proportional to the logarithm of the total flux, including the rf fields and collisions. (c) Contours of the electron distribution function for the case of figure 8 for 1 MW of power.

(d) Same as (c) but for 10 MW of power. In (c) and (d) the contours span 12 orders of magnitude, and the axes are momentum per rest mass normalized to a normalizing velocity vnorm.

Fig. 10. (a) Driven current per unit power as a function of the ratio of density to electron temperature at the mid-radius, for calculations similar to that of figure 4, but using scaled density and temperature profiles; (b) normalized minor radius where the driven current peaks as a function of β_e at the mid-radius. The plus symbols are for the T_e scan, the diamond symbols are for the n_e scan, and the squares are for the scan of both T_e and n_e.

Fig. 11. Ray data plotted as a function of the poloidal projection of the ray trajectory, for launched $n_{||}$ of 3.0 (left) and 4.0 (right) for the case of figure 4. The top row of boxes are the electron temperature and $n_{||}/2$; the middle boxes are the power P remaining in the ray, the derivative $-dP/ds$ showing the rate of power absorption, and the normalized minor radius r; and the bottom boxes show the local value of $v_{||}/v_{te} = \xi_e$. In both cases, the vertical dotted line indicates the location of the peak rate of attenuation.

Fig. 12. Equilibrium for FNSF. The plasma current is 6.6 MA, the toroidal field is 5.44 T. The vertical lines are harmonics of the deuterium cyclotron frequency for an applied frequency of 1.2 GHz. The central ray is shown for $n_{||}$=2.2 launched at $\rho = 0.98$. The thickness of the central ray is proportion to the power deposition per unit ray length.

Fig. 13. (a) Profiles of electron density and temperature and (b) safety factor, for the FNSF equilibrium of figure 12.

Fig. 14. Profile of driven current by 1 MW of fast wave power at 1.2 GHz with launched $n_{||}$ of 2.2, for the FNSF equilibrium of figure 12 and profiles of figure 13. The solid line

is for GENRAY and the dashed line is for CQL3D. The integrated current is 37.7 kA from GENRAY and 34.9 kA from CQL3D.

Fig. 15. Same data as figure 11, but for FNSF with $n_{||}$ (a) of 1.8 on the left and 2.6 on the right.

Fig. 16. Spectrum of $n_{||}$ for a combline antenna at 500 MHz and of length 1.8 m. The solid curve has no plasma loading, the dashed curve has 90% damping by the antenna end. The center of the spectrum is $n_{||}$=3.0.

List of Figures

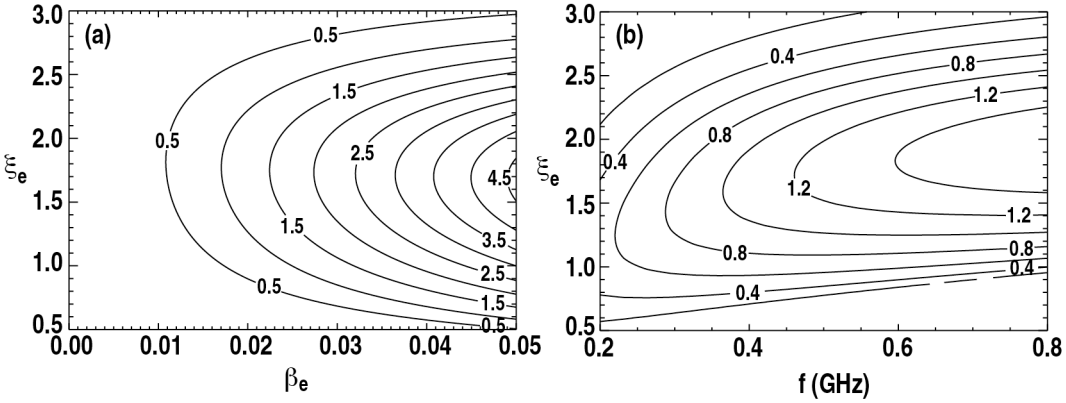

R. Prater, Fig 1

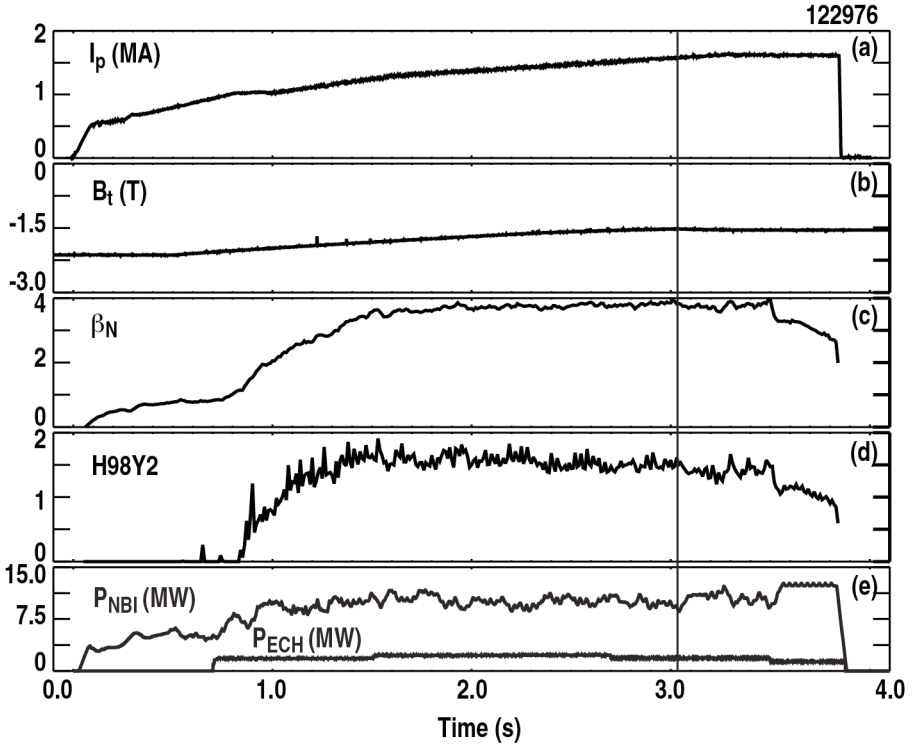

R. Prater, Fig 2

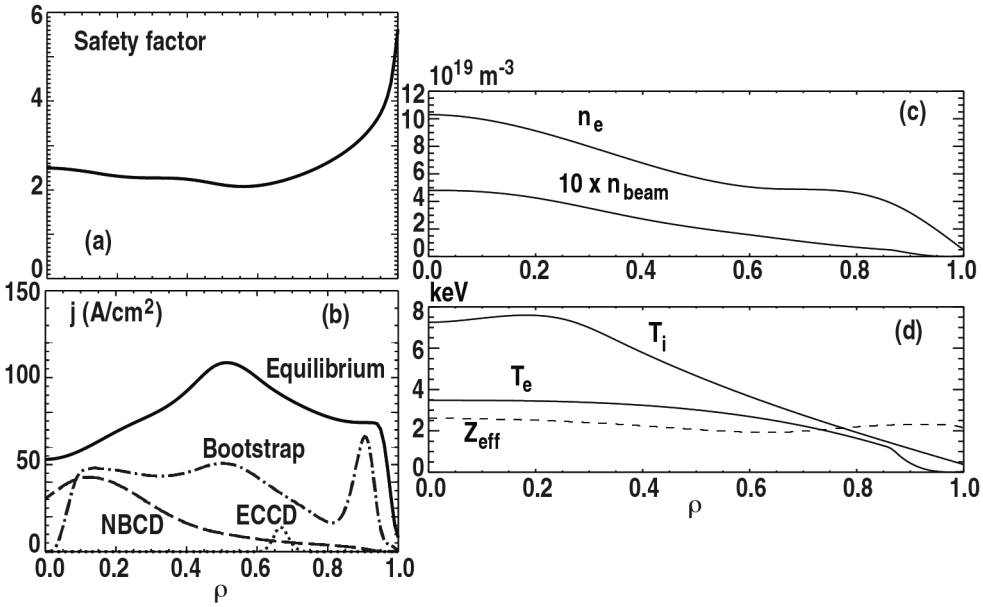

R. Prater, Fig 3

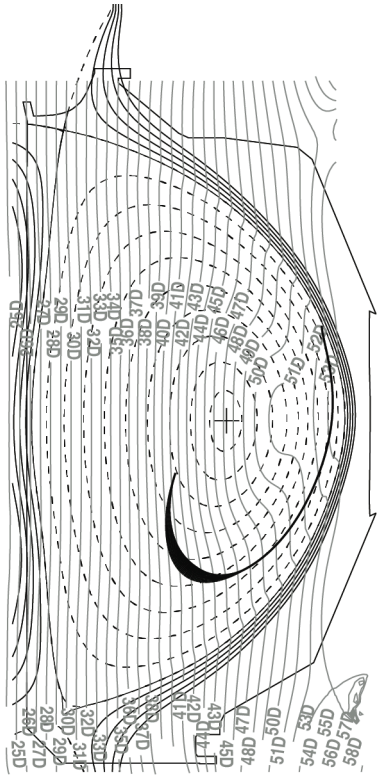

R. Prater, Fig 4

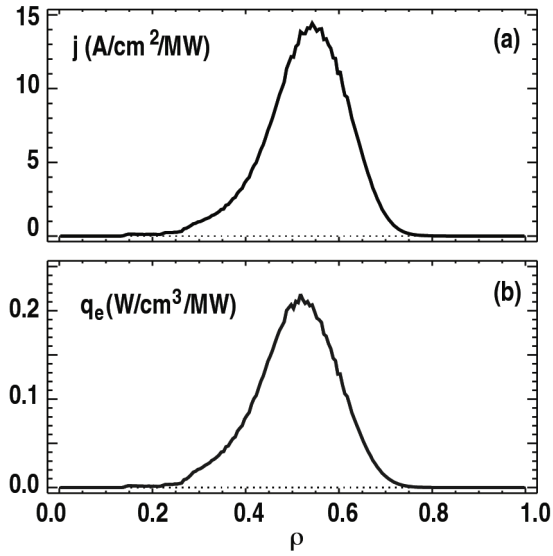

R. Prater, Fig 5

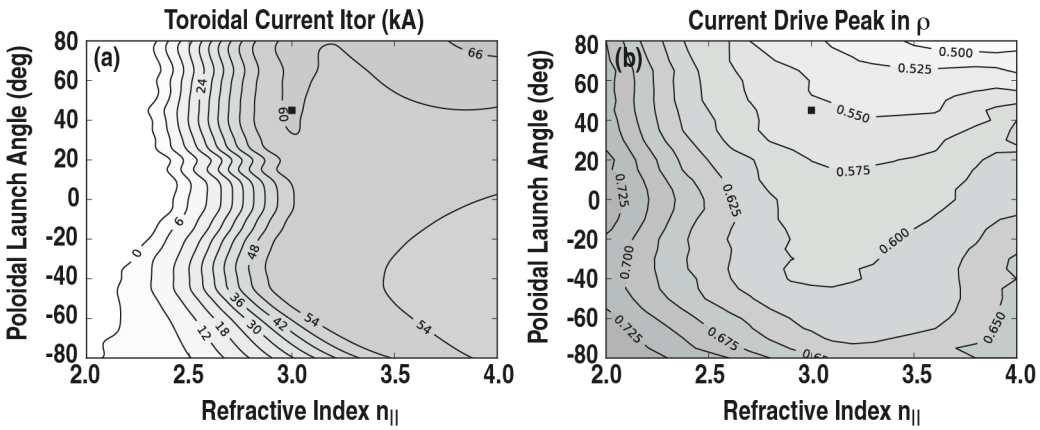

R. Prater, Fig 6

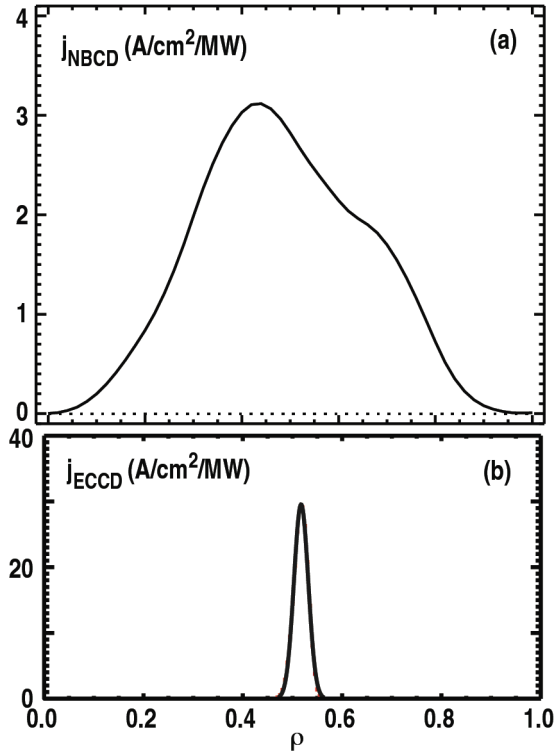

R. Prater, Fig 7

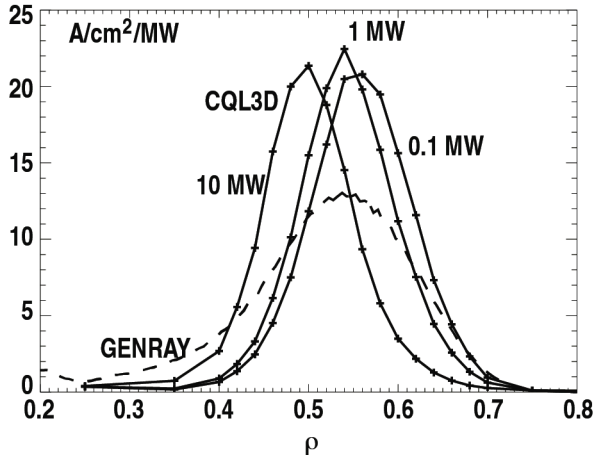

R. Prater, Fig 8

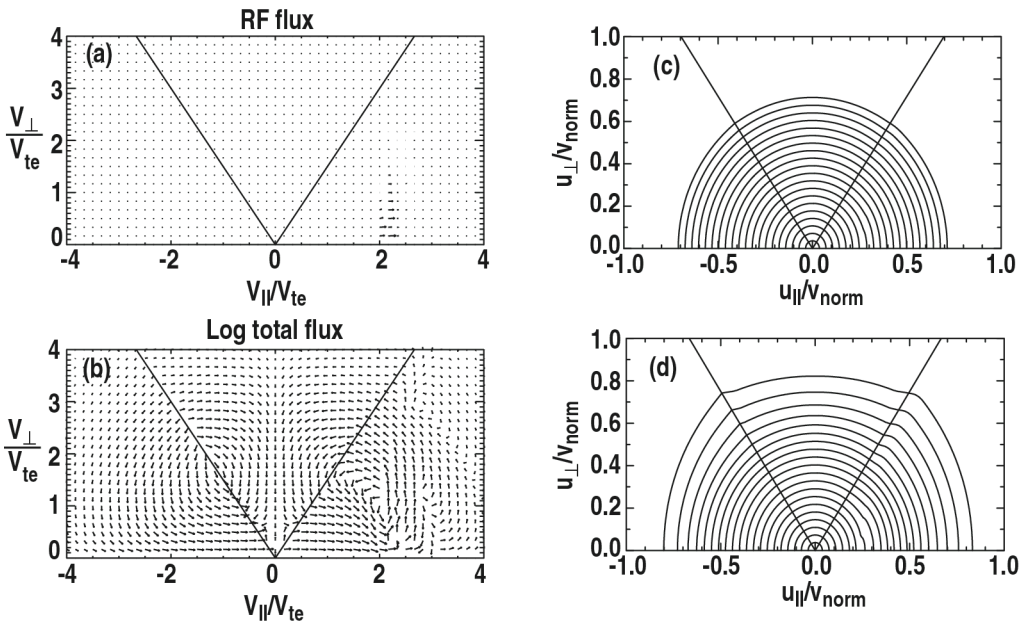

R. Prater, Fig 9

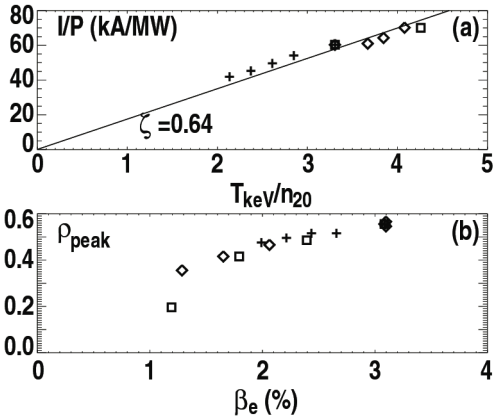

R. Prater, Fig 10

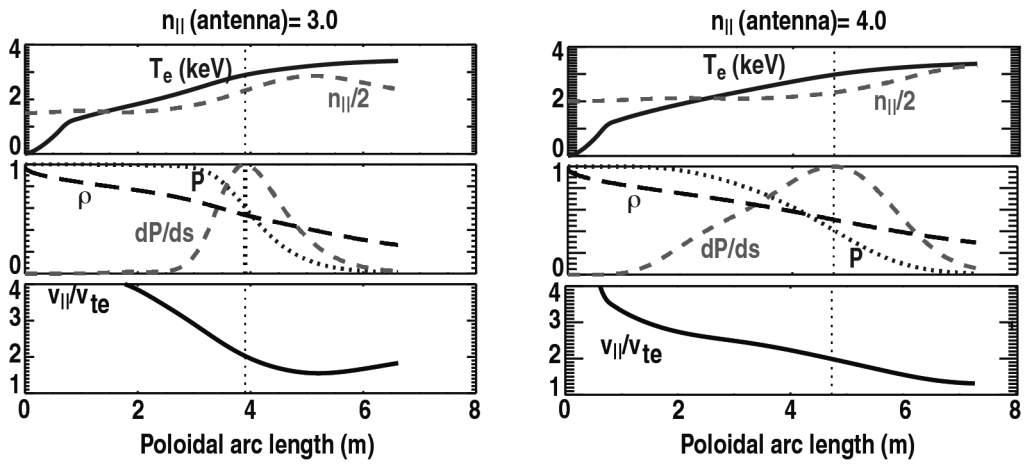

Prater, Fig 11

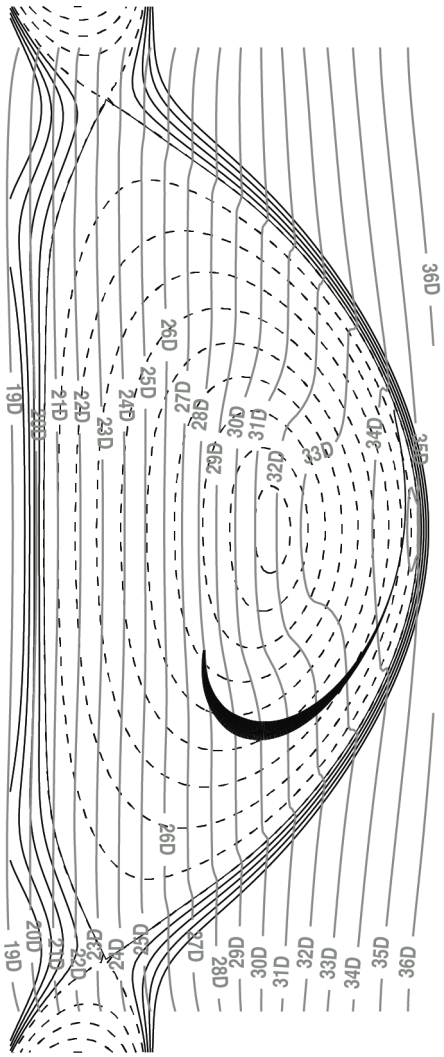

R. Prater, Fig 12

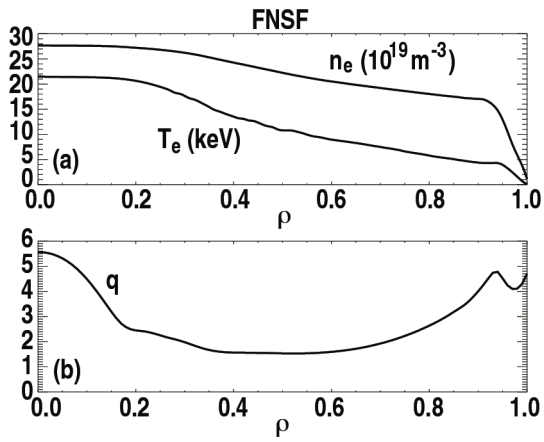

R. Prater, Fig 13

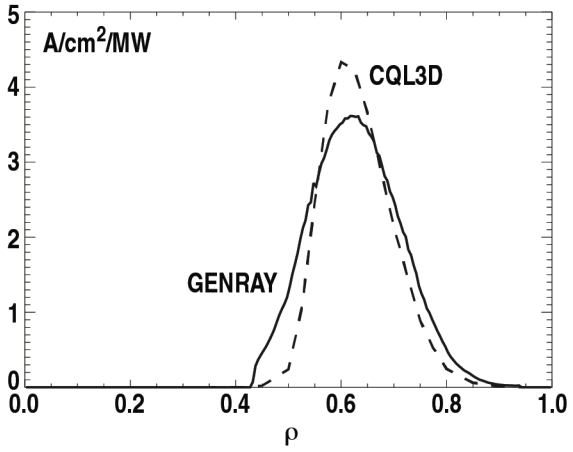

R. Prater, Fig 14

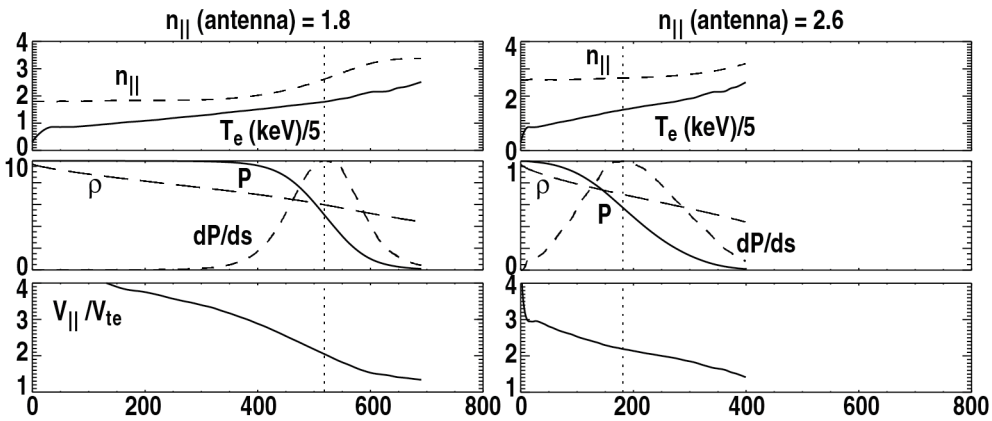

R. Prater, Fig 15

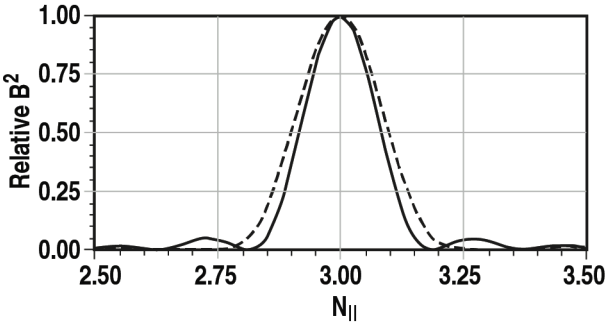

R. Prater, Fig 16